iScience

CellPress
OPEN ACCESS

Article

Working memory expedites the processing of visual signals within the extrastriate cortex

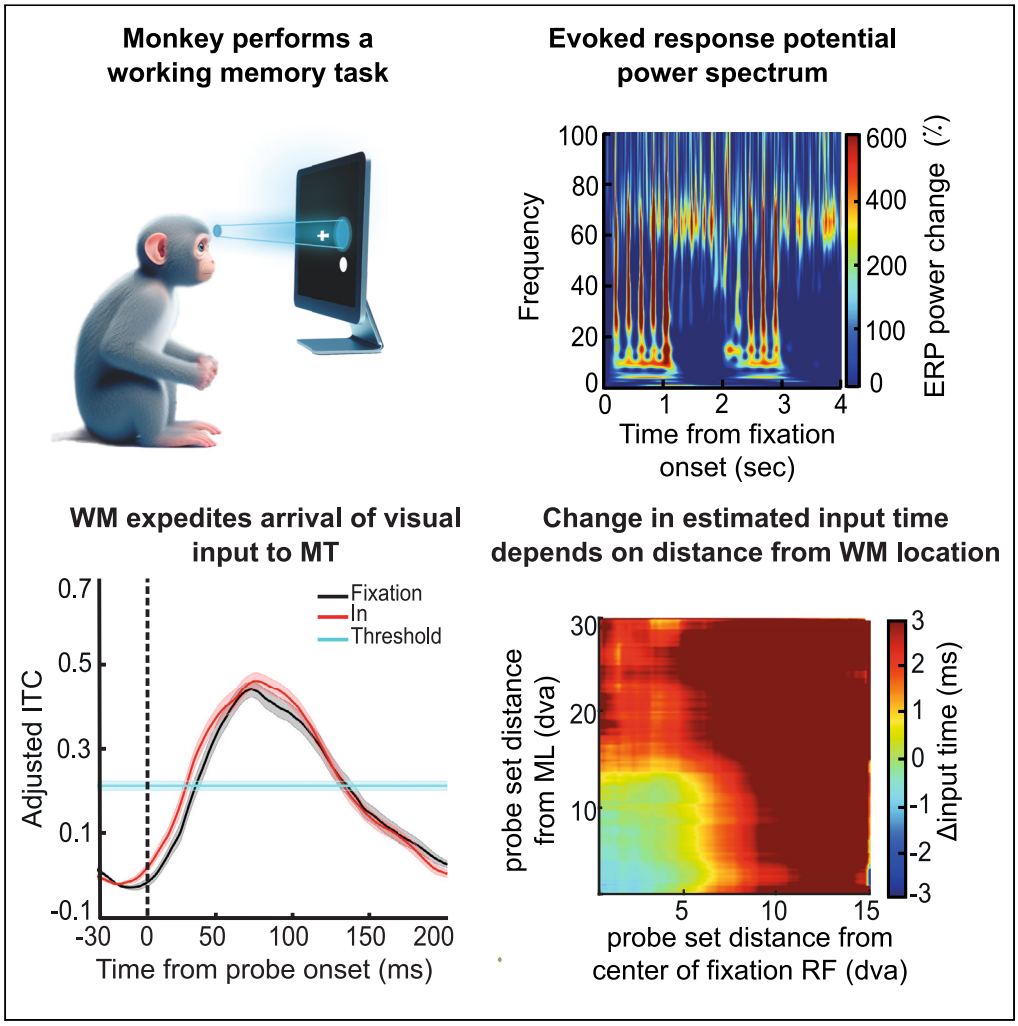

Majid Roshanaei, Zahra Bahmani, Kelsey Clark, Mohammad Reza Daliri, Behrad Noudoost

zabahmani@gmail.com (Z.B.)
daliri@iust.ac.ir (M.R.D.)
behrad.noudoost@utah.edu (B.N.)

Highlights

Different methods for measuring onset of visual responses are compared

The arrival time of visual input is quantified using inter-trial coherence

Visual input to MT arrives earlier at the location held in working memory

Roshanaei et al., iScience 27, 110489
August 16, 2024
https://doi.org/10.1016/j.isci.2024.110489

iScience

CellPress
OPEN ACCESS

Article

Working memory expedites the processing of visual signals within the extrastriate cortex

Majid Roshanaei,[1] Zahra Bahmani,[2,*] Kelsey Clark,[3] Mohammad Reza Daliri,[1,*] and Behrad Noudoost[3,4,*]

SUMMARY

Working memory is the ability to maintain information in the absence of sensory input. In this study, we investigated how working memory benefits processing in visual areas. Using a measure of phase consistency to detect the arrival time of visual signals to the middle temporal (MT) area, we assessed the impact of working memory on the speed of sensory processing. We recorded from MT neurons in two monkeys during a spatial working memory task with visual probes. When the memorized location closely matches the receptive field center of the recording site, visual input arrives sooner, but if the memorized location does not match the receptive field center then the arrival of visual information is delayed. Thus, working memory expedites the arrival of visual input in MT. These results reveal that even in the absence of firing rate changes, working memory can still benefit the processing of information within sensory areas.

INTRODUCTION

Working memory is the capacity to maintain information in order to guide our actions,[1] and is correlated with overall cognitive ability.[2,3] At a behavioral level, working memory alters discrimination thresholds,[4] and produces attention-like reaction time benefits in responses to visual stimuli matching the content of working memory.[5] Some studies have shown that working memory can interfere with or distort the perception of new stimuli, especially when they share features or dimensions with the memorized information.[6] Other studies have shown that individual variability in working memory is related to the regulation of emotional stimuli, depending on their valence and relevance.[7] Moreover, working memory can also be affected by stimulus processing, as incoming stimuli can create bias or noise in the representation of the memorized information.[8] These behavioral effects of working memory in stimulus processing reflect the shared neural mechanisms underlying the maintenance and manipulation of information in the brain.

There are multiple ongoing debates regarding the exact nature and location of working memory maintenance. One dispute is the relative contributions of higher-order prefrontal and parietal vs. sensory areas. Persistent spiking activity reflecting the content of working memory was long assumed to be a hallmark of an area's involvement in working memory maintenance[9]; arguing against the involvement of sensory areas, neurons in visual areas generally have weak or no modulation during working memory maintenance.[10–16] For instance, neurons in earlier visual areas, like the V4 and middle temporal (MT) cortex, exhibit little change in their firing rate during the delay period of working memory tasks,[13,14] and a working memory-dependent change in spiking activity emerges later in the visual hierarchy.[12] However, multiple fMRI studies have shown that the content of working memory can be decoded from various sensory areas.[17–21] Behavioral experiments examining the effect of masks and stimulus position also suggest a contribution of visual areas to memory performance,[22,23] and prefrontal activity comparing remembered items to the current sample depends upon the degree of overlap in earlier cortical areas.[24] Indeed, some studies have reported modulation of V1 firing rates by working memory,[16,25] and multiple cognitive factors alter MT responses throughout all phases of the memory task.[26] More recently, the necessity of persistent activity in individual neurons reflecting the content of working memory throughout the delay has been called into question, with proposals for activity-silent mechanisms based on synaptic plasticity,[27–29] or dynamic activity patterns shifting across individual neurons throughout the delay within prefrontal areas.[30,31] These are active topics of research,[32–38] and multiple reviews attempt to synthesize and reconcile these findings.[39–44] Our own research shows that in area MT, working memory increases the power of alpha-beta oscillations without changing average firing rates,[45] indicating the existence of a subthreshold top-down input that may alter subsequent visual processing.

Rather than focus on this question of the neural correlates of memory maintenance, we instead look for changes in the neuronal response to incoming visual signals during working memory. These changes presumably underlie the enhancement of visual stimuli at the location held in spatial working memory.[4,5] Our own previous work[45–47] has identified some changes in visual responses during working memory, using the same dataset analyzed in this study. Recording from the MT cortex, we found no changes in baseline firing rates during memory

[1]Biomedical Engineering Department, School of Electrical Engineering, Iran University of Science and Technology (IUST), Narmak, P.O. Box 16846-13114, Tehran, Iran
[2]Department of Electrical & Computer Engineering, Tarbiat Modares University, Tehran 1411713116, Iran
[3]Department of Ophthalmology and Visual Sciences, University of Utah, Salt Lake City, UT 84132, USA
[4]Lead contact
*Correspondence: zabahmani@gmail.com (Z.B.), daliri@iust.ac.ir (M.R.D.), behrad.noudoost@utah.edu (B.N.)
https://doi.org/10.1016/j.isci.2024.110489

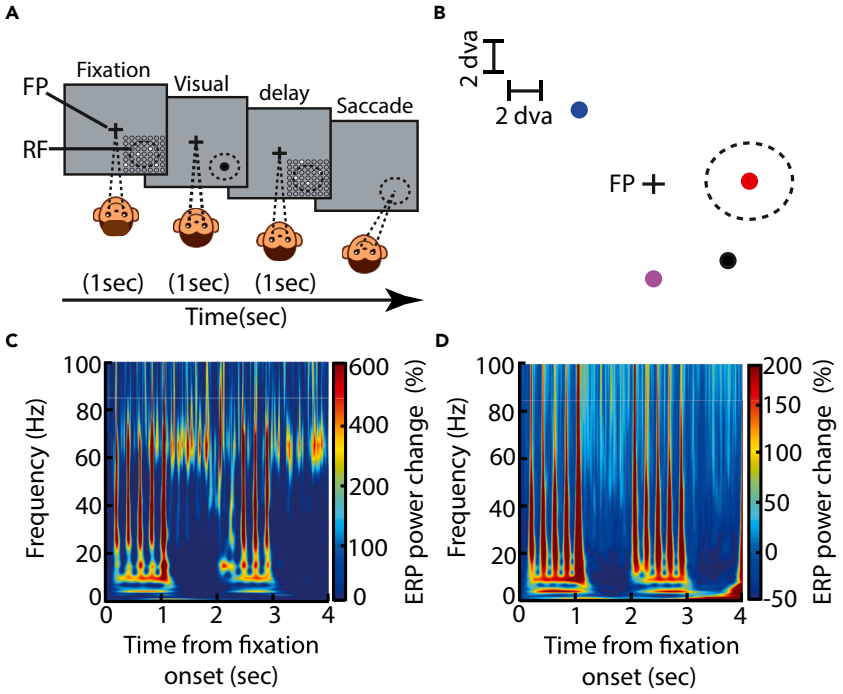

Figure 1. Working memory task and evoked response potential power spectrum

(A) Schematic of the memory guided saccades (MGS) task with visual probes. The animal fixates at the center of the screen for 1 s, during which four visual probes appear sequentially (200 ms duration, ~1 d.v.a; 7 × 7 grid of possible probe locations shown). A visual cue stimulus appears for 1 s in one of four possible locations (shown in Figure 1B); the monkey maintains fixation while remembering this location for 1 s, during which another four visual probes are presented. When the fixation point (FP) disappears, the monkey saccades to the remembered cue location to receive a reward.

(B) Four possible locations of the visual cue (colored dots) relative to the estimated receptive field (dashed line). Scale bars in upper left show degrees of visual angle (dva).

(C) Evoked response potential power change (relative to pre-stimulus baseline) over time and frequencies for an example recording channel.

(D) Evoked response potential power change (relative to pre-stimulus baseline) over time and frequencies averaged across 288 recorded channels.

maintenance,[45] but changes in visually evoked firing rates and shifts in receptive fields resulted in increased spatial discriminability for stimuli near the remembered location.[46] Similar enhanced visual responses for stimuli matching the content of object working memory have been observed with fMRI.[48] Interneuronal correlations in MT visual responses were also modulated by the content of working memory.[47] Local field potential (LFP) power was altered at the remembered location, as were times of visually evoked spikes relative to those LFP oscillations.[45] Here, we extend our analysis of the impact of working memory on visual processing to examine when visual information first arrives in MT.

Does working memory also drive changes in the timing of visual signals? By analyzing spiking activity and LFPs from sites within the MT cortex during a spatial working memory task, we investigated the impact of working memory on the speed with which visual input reaches MT. We measured the receptive fields in the MT cortex and varied the locus of working memory relative to each receptive field, and assessed the time of arrival of the stimulus-induced synaptic inputs to MT. We used inter-trial coherence (ITC), which quantifies the phase locking of the LFP across trials, to sensitively capture both phase-locked LFP amplitude changes and phase resets.[49] Our investigation revealed that if the memorized location closely matches both the stimulus location and the neurons' receptive field center, visual input arrives in MT sooner; on the other hand, if the memorized location is far from the stimulus location or the receptive field center, then the arrival of visual information is delayed. These results reveal that working memory can improve the speed with which visual signals arrive in sensory areas, supporting the idea that working memory recruits sensory areas.[50]

RESULTS

In order to study the impact of working memory on the speed of visual processing, we recorded spiking and LFP activity from the MT cortex of two monkeys using 16-channel linear array electrodes (205 multi-units, 137 isolated single units, and 288 LFP channels over 18 recording sessions). The animal performed a spatial working memory task with task-irrelevant visual probes (Figure 1A). The monkey was presented with a visual cue and had to remember the cued location throughout a delay period, and then make a saccadic eye movement to the memorized location to receive a reward. 200-ms visual probes were presented near the neuron's receptive field during the fixation and delay periods. Each neuron's receptive field was assessed based on its firing rate in response to a 7 × 7 matrix of probes presented during the fixation period of the task (see STAR Methods). The memorized location could be in various positions relative to the neuron's receptive field (Figure 1B). For

each neuron, "memory In" refers to the condition where the memory location was within the receptive field of that neuron (the red dot in Figure 1B). Note that there were three potential memory locations in or near the estimated MT receptive field (black dashed line in Figure 1B; purple, red, and black dots), with the "memory In" condition assigned after recordings to the condition with its target closest to the receptive field center (see STAR Methods). The condition in which the memory location was in the opposite visual hemifield from the memory In location is called the "memory Out" condition (the blue dot in Figure 1B). The condition with the memory location farthest from the receptive field while still being in the same hemifield is called the "memory Flank" condition (the purple dot in Figure 1B). To determine how holding a location in working memory alters visual processing, we assessed the spiking and LFP activities in response to visual probes and studied how the deployment of working memory alters these visually evoked activities. The evoked response potential is measured as the average of LFPs across trials. As the first step, we assessed the power spectrum of the evoked response potentials over time (Figures 1C and 1D). This method revealed evoked LFP activity in response to both the visual cue and the visual probes (Figures 1C and 1D). Figure 1C shows the percentage of evoked response potential power change relative to the baseline period (150 ms following initial fixation) for an example recording channel. This power spectrum revealed a consistent gamma (>30 Hz) component following the visual cue, as well as an alpha-beta (5–25 Hz) component in response to probes during the fixation and delay periods. Figure 1D displays the percentage of evoked response potential power change relative to baseline, averaged across all 288 recorded channels. Both alpha-beta (5–30 Hz) and gamma (30–70 Hz) frequency components were modulated in response to the presentation of probes and the visual cue (%power change $_{\text{alpha-beta}}$ = 298.90 $\pm$ 8.74, $p < 10^{-48}$; %power change $_{\text{gamma}}$ = 481.00 $\pm$ 24.20, $p < 10^{-48}$, n = 288 LFP channels).

To measure the impact of working memory on the time when visual input reaches MT, we first measured the latency of the neurons' response to their optimal probes based on their average firing rates or their probe-evoked LFPs. The optimal probes are defined as probes with an evoked firing rate response of more than 60 percent of the maximum response of the neuron to all probes. The results for an example recording channel are shown in Figure 2. Figure 2A shows the example neuron's receptive field profile. The neuron's firing rate in response to the presentation of its optimal probe is shown in Figure 2B, when the probe is presented during fixation or the delay period of the memory In and Out conditions. For this sample neuron, the time at which the neuron's firing rate exceeds the baseline was not different across conditions (50 ms for all three conditions). Across the population, we did not find a significant difference in the time at which the firing rate of MT neurons signaled the presence of the probe in their receptive field between memory and Fixation conditions (Figures S1A and S1B; the time that firing rate differs from its baseline: memory In = 44.02 $\pm$ 1.37 ms, Fixation = 45.62 $\pm$ 1.36 ms, p = 0.105, n = 75 neurons). Figure 2C illustrates the evoked response potential from the same recording channel as in Figures 2A and 2B in response to the same visual probe. Similar to the average spiking activity, the time at which the evoked response potential response to the probe began to change was not different between the Fixation and memory In and Out conditions, either for this example neuron (the time that evoked response potential differs from its baseline: Fixation = 54 ms, memory In = 53 ms, memory Out = 53 ms), or for the population (memory In = 58.54 $\pm$ 2.94 ms, Fixation = 55.37 $\pm$ 2.02 ms, p = 0.779, n = 75 neurons; Figure S2A). Therefore, assessing the time of visual signal arrival based on spiking activity or raw LFP fluctuations did not reveal any impact of working memory on the processing of sensory signals.

ITC of the LFP is a proxy for estimating the timing of the signal-induced synaptic inputs (see STAR Methods), which may be more sensitive than raw LFP or spiking measurements. Phase-locked LFP amplitude variations and phase resets are sensitively captured by ITC, which measures the LFP's phase locking across trials. Since we observed that the evoked response potential after probe onset is dominated by an alpha-beta band component (Figure 1D), we measured the ITC in the 5–25 Hz range. We adjusted the ITC for each condition by subtracting the average of ITC values within the 30 ms prior to probe onset (see STAR Methods for details). We set a threshold equal to the randomly sampled ITC for each neuron. Estimated input time (EIT) is measured as the time at which the adjusted ITC significantly exceeded the threshold (see STAR Methods). Figure 2D shows the ITC for the Fixation and memory conditions for the same recording channel characterized in Figures 2A–2C. For this sample channel, the Fixation, memory In, and memory Out conditions had slightly different EITs: the EIT was shorter during the memory In condition compared to the memory Out or Fixation conditions (EIT_{In} = 44 ms, EIT_{Out} = 51 ms, $EIT_{Fixation}$ = 55 ms). Figure 2E shows the average adjusted ITC and the average threshold during the memory In and Fixation conditions for the population of 75 channels with neurons whose receptive field centers were close to the memorized location. Across the population, EITs were faster for memory In compared to Fixation (Figure 2F; EIT_{In} = 36.31 $\pm$ 1.71 ms, $EIT_{Fixation}$ = 41.45 $\pm$ 1.98 ms, p = 0.003, n = 75 channels), but there was no significant difference between memory Out and Fixation (EIT_{Out} = 39.77 $\pm$ 1.72 ms, p = 0.160, n = 75 channels). These findings were also true in a larger population of LFP sites (n = 131 channels selected based on receptive fields defined by multi-unit activity; Figure S3). EITs were shorter for memory In compared to Fixation (EIT_{In} = 36.67 $\pm$ 1.22 ms, $EIT_{Fixation}$ = 39.58 $\pm$ 1.24 ms, p = 0.001, n = 131 channels), and there was no significant difference between memory Out and Fixation (EIT_{Out} = 38.36 $\pm$ 1.35 ms, p = 0.146, n = 131 channels). Comparing the ability of the ITC, firing rate, and ERP-based methods for estimating input time to differentiate between artificial shifts in the latency of the data, the sensitivity of ITC and firing rate-based methods appeared comparable (Figure S4), suggesting that this may be a decrease in the latency of input arrival in MT without a change in the latency of spiking. Thus, remembering a location speeds up the arrival of incoming visual input at MT sites with a receptive field center closely matching the memorized location.

The impact of memory on input arrival time was quite different for sites with neurons whose receptive field centers were farther from the memorized location (Figure 3). For the population of recorded neurons, we called the condition when the memory cue appeared at the flank of the neuron's receptive field the "Flank condition" (see STAR Methods). Figure 3A shows the receptive field of a sample neuron and the location of the memorized target at its flank. The neuron's EIT, calculated based on ITC, is shown in Figure 3B: EIT was later for the Flank condition compared to memory Out or Fixation (EIT_{Flank} = 53 ms, EIT_{Out} = 46 ms, $EIT_{Fixation}$ = 46 ms). Figure 3C shows the mean ITC in the Flank and Fixation conditions for all recorded channels (n = 137 channels). Figure 3D compares the EIT for memory Flank and Out vs.

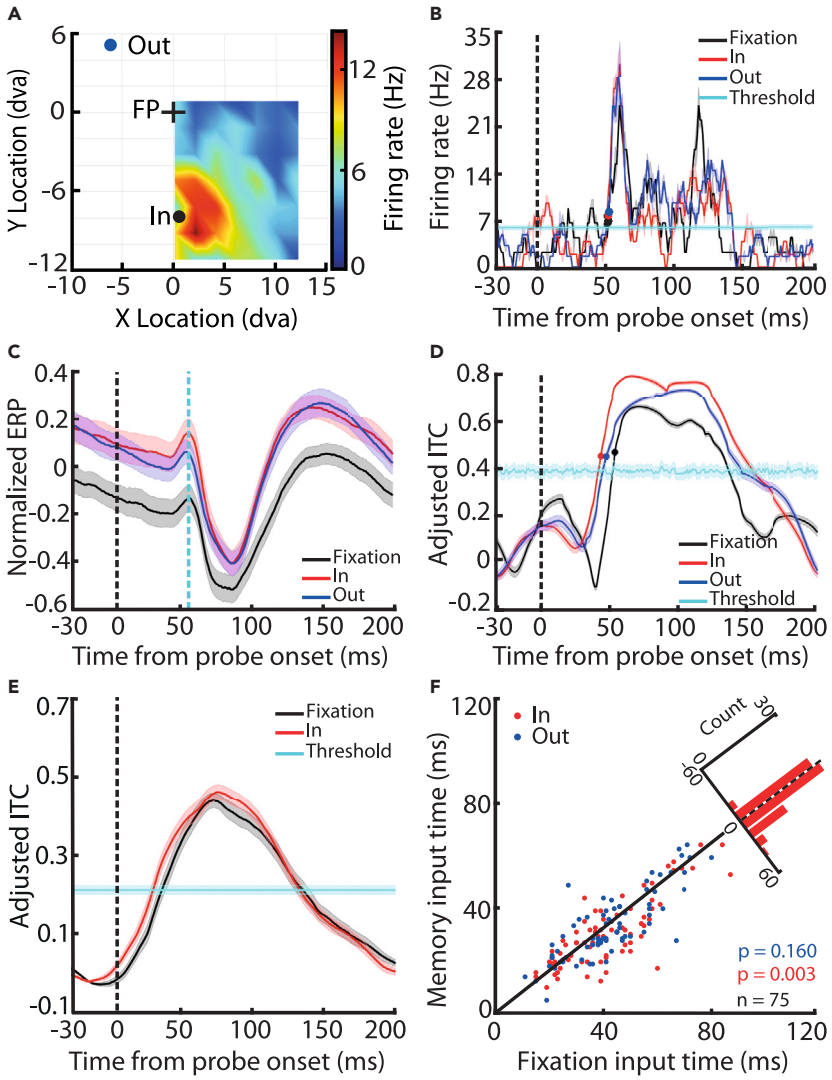

Figure 2. EIT based on firing rate, evoked response potential, and ITC

(A) The receptive field of a sample MT neuron and the relative position of the visual cue for the memory In and Out conditions (black and blue dots).

(B) Firing rate of the sample neuron in response to optimal probes over time, during Fixation (black), memory In (red), and memory Out (blue). The cyan line represents the baseline firing rate (grand average response across time and trials). In B-E, shading shows standard error.

(C) Evoked response potential was calculated from the LFP at the same site as the sample neuron, in response to visual probe onset for the same conditions. Vertical cyan line shows time when evoked response potential differs from baseline.

(D) Adjusted ITC over time for the same LFP site, during Fixation (black), memory In (red), and memory Out (blue). The cyan line shows the randomly sampled ITC, and the dots on each ITC trace indicate when the ITC for that condition significantly exceeded that value (the EIT; see STAR Methods).

(E) Adjusted ITC measure for the population of MT sites with neurons whose receptive field centers were close to the visual cue location ($n = 75$), for memory In (red) and Fixation (black).

(F) The scatterplot of EIT for memory In (red) and Out (blue) vs. Fixation across all recorded channels. The histogram in the upper right shows the distribution of memory In and Fixation differences across channels. *p*-values compare fixation to memory input times.

Fixation across these 137 channels. EITs for memory Flank were significantly longer than for Fixation ($EIT_{Flank} = 41.51 \pm 1.25$ ms, $EIT_{Fixation} = 39.24 \pm 1.24$ ms, $p < 10^{-3,}$ $n = 137$ channels). EIT for memory Out was also slightly longer than for Fixation ($EIT_{Out} = 39.72 \pm 1.26$ ms, $p = 0.020$, $n = 137$ channels; see also Figure S5). Thus, whereas remembering a location speeds up the arrival of visual input when the memorized location matches the receptive field of neurons, it delays the arrival of visual information when the locus of memory is farther from the neuron's receptive field. In contrast to the ITC method, calculations of input time based on the firing rate generally failed to find any significant differences for either the In or Flank conditions (Figure S1). We also calculated EIT based on when the ITC reached 50% of its maximum value and found the same results (Figure S6). Phase variance drops after probe onset (see STAR Methods), and the basic findings were also replicated when calculating EIT based on when the phase variance across trials reached 50% of its minimum (Figure S7).

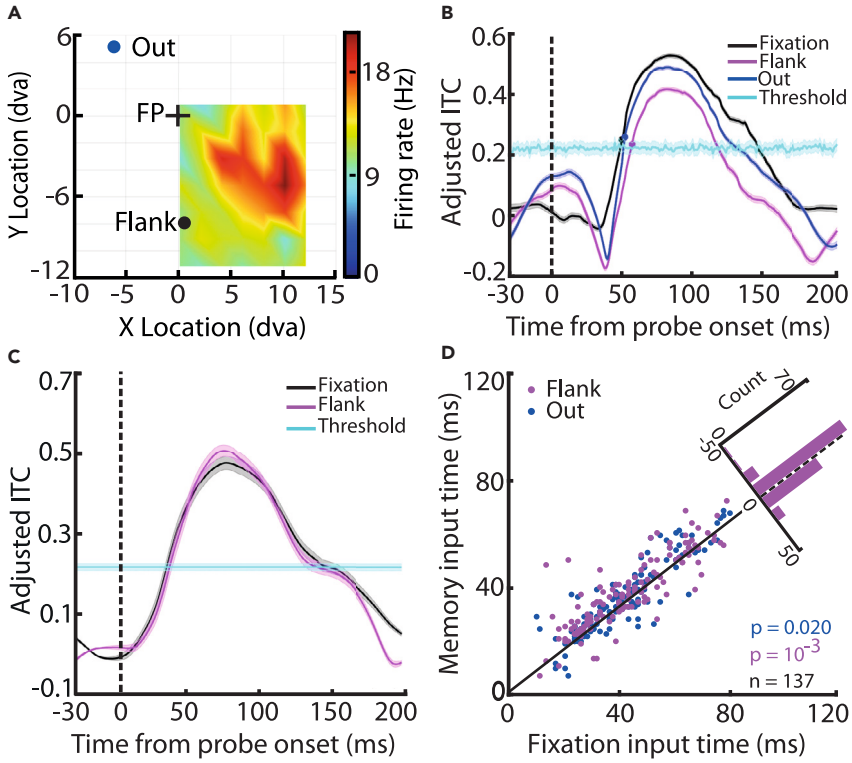

Figure 3. Working memory increases EIT for sites with receptive fields further from the memorized location

(A) The receptive field of an example neuron with a receptive field center farther from the memorized location (black dot).

(B) Adjusted ITC over time for the LFP from the same site as the example neuron in (A), for Fixation (black), memory Flank (purple), and memory Out (blue) conditions. Dots show when each trace became significantly different than the randomly sampled ITC (cyan line; $p < 0.05$).

(C) The population mean ITC in the Flank (purple) and Fixation (black) conditions across all recorded channels ($n = 137$; shading shows SE).

(D) The scatterplot of EIT for memory Flank (purple) and Out (blue) vs. Fixation across all recorded channels. Histogram in the upper right shows the distribution of memory Flank and Fixation differences. *p*-values compare fixation and memory input times.

Having observed differences in the effect of memory on input time for sites with receptive fields classified as either close to or far from the memorized location, we next sought to more fully characterize the impact of distance between the receptive field center and the memorized location on input time. We estimated the input time as a function of the visual probe's distance from both the receptive field center and the memorized location (pooling responses for 4 neighboring probe locations as illustrated in Figure 4A). The difference in EIT between the memory and Fixation conditions, as a function of probe distance from the receptive field center and memorized location, is shown for the population of 342 LFP sites (with receptive fields defined by single- or multi-unit recordings) in Figure 4B (sample size across the various location combinations of Figure 4B is shown in Figure S8). When the probe appeared close to both the receptive field center and the memorized location, EIT decreased in the memory condition; when the probe was far from either the receptive field center or the memorized location, EIT increased compared to Fixation. We fit a polynomial to predict memory EIT given Fixation EIT and distance from the receptive field center and memorized location (see STAR Methods). Figure 4C shows input times predicted by a polynomial model that was fitted to the data in Figure 4B (coefficients in Methods; R-squared = about 0.33). Overall, the results show a synergistic interaction between the proximity of the probe to the receptive field center and the memorized location, with the greatest improvement in input speed occurring for visual stimuli presented at the receptive field center while the same location is held in working memory.

DISCUSSION

We found that the ITC method provided a more sensitive measure of input arrival time than average firing rates or LFPs. Moreover, our study revealed the effect of working memory on how quickly visual input arrives in MT. It also showed the dependence of this working memory effect on the relative distance of the working memory locus and neuronal receptive field: if the memorized location closely matches the receptive field center of the recording site, visual input arrives in MT sooner, but if the memorized location does not match the receptive field, then the arrival of visual information is delayed. We also showed that if visual stimuli are located far from either the receptive field center or the memorized location, then the arrival of visual input in MT is delayed; if visual stimuli are close to both the receptive field center and the memorized location, visual information arrives sooner. Thus, we find that working memory expedites the arrival of sensory information in MT at sites representing the memorized location.

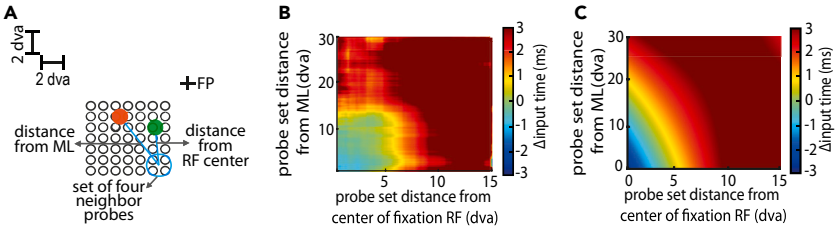

Figure 4. Spatial profile of changes in EIT

(A) Schematic showing how four neighboring probes are pooled when calculating the distance from the memorized location (ML; orange dot) and the receptive field center (green dot). Scale bars in upper left indicate dva.

(B) Difference between EIT for memory vs. Fixation, as a function of the probe distance from the site's receptive field (RF) center (x axis) and the memorized location (y axis), across the population of 342 recording sites. Receptive field centers were measured based on single- or multi-unit activity recorded at the site.

(C) Input time from a fitted polynomial model (R-squared = 0.33; coefficients in Methods).

One remaining question is the mechanism by which this working memory-driven earlier arrival of visual input occurs. One possibility is that the areas providing input to MT might themselves have faster latencies at the memory location. Similarly, delayed input to other locations might reflect delays in earlier areas or disadvantageous changes in spike timing; it is also possible that this apparent delay results from a shift in frequency or aperiodic processing without actually delaying input time. Further experiments examining visual responses earlier in the visual hierarchy during working memory will be needed to ascertain the origin of the change in the time of input arrival.

We have been hypothesizing that the changes in MT responses are related to enhanced perception of visual stimuli matching the content of working memory, as has been reported behaviorally.[4,5] However, it is possible that some of the changes in visual responses serve a different purpose: multiplexing information to prevent interference between visual and remembered stimuli. Such segregation of multiple remembered items by oscillatory phase was recently reported by Abdalaziz et al., who showed that different working memory items are associated with different phases of EEG oscillations.[51] This strategy, which is a form of time-division multiplexing, could prevent representational conflict between working memory items by allocating them to non-overlapping time slots. This concept is similar to one proposed for the sensory representation of multiple objects, in which the sensory cortex can use time-division multiplexing to represent multiple stimuli.[52,53] Extending this idea to our own results, a similar phase-based mechanism could be used to prevent interference between one working memory item and a presented visual stimulus. In this framework, the consistency of the visually evoked phase in the current study could be interpreted as a temporal "window of opportunity" for visual processing, distinct from phases dedicated to working memory maintenance.

Another question is how these latency changes are related to the behavioral benefits of working memory in responding to certain stimuli. We cannot exclude the possibility that the changes in input arrival times are ultimately reflected in spiking latencies, at least for some subset of MT neurons (although we failed to find such a change in spiking latency across the MT population), eventually contributing to faster reaction times. Another possibility is that this earlier arrival of input, with no change in the timing of the first visually driven spikes in MT, results in an increase in processing time, and this increased processing time is beneficial for the MT spiking representation. This increased processing time might contribute to increased gain or discriminability of MT spiking responses at the memory location which have been reported in this dataset,[46] by allowing a longer window for integrating information. In the current dataset, we are not able to address whether there is an influence of visual stimuli appearing during working memory maintenance on that maintenance. Although the memory-guided saccade task has often been used to study spatial working memory,[54,55] we cannot exclude the possibility that the observed change in input time is related to motor preparation.[56]

There is a large degree of overlap between the neurophysiological signatures of spatial attention and spatial working memory in visual areas[57]; our finding of faster arrival of visual input to MT at the location held in working memory adds another example to the list of similarities. Some of the neural signatures of attention in visual cortex are increased firing rates, enhanced tuning properties, reduced variability, shifts in receptive fields, and changes in inter-neuronal correlations (reviewed by Noudoost et al.[58]). Similarly, in the same dataset as the current study, working memory has been reported to shift receptive fields,[46] increases visual responses,[45,46] decrease variability,[46] and alter inter-neuronal correlations.[47] Changes in oscillatory power and coherence have also been reported during both working memory[12,59–62] and attention,[63–69] particularly in the alpha/beta and gamma frequency bands. Several theories have been proposed to offer explanations for the functional relevance of these oscillatory changes for attention[70–72] and working memory.[50,73,74] Covert spatial attention has also been reported to decrease latencies of neuronal responses in both V4[75] and MT,[76] as well as in V1 for overt shifts of attention,[77] with the findings reported here providing another point of similarity. These shared signatures imply that working memory and attention are closely related neural processes that rely on tightly linked coding and control mechanisms in the brain.

Limitations of the study

We hypothesized that working memory would influence processing across the visual hierarchy, including MT, as demonstrated in our findings. Future research will be needed to determine how changes in upstream areas contribute to the observed change of input arrival time in MT, how the timing or information content of MT output is affected by this change in arrival time, and how these changes impact visual processing in areas further up the visual hierarchy.

STAR★METHODS

Detailed methods are provided in the online version of this paper and include the following:

- KEY RESOURCES TABLE
- RESOURCE AVAILABILITY
  - Lead contact
  - Materials availability
  - Data and code availability
- EXPERIMENTAL MODEL AND STUDY PARTICIPANT DETAILS
  - General and surgical procedures
  - Behavioral monitoring
  - Behavioral tasks
  - Neurophysiological recording
- METHOD DETAILS
  - Data analysis
  - ITC method
  - EIT calculations
  - Phase variance
  - Fitted model
- QUANTIFICATION AND STATISTICAL ANALYSIS

SUPPLEMENTAL INFORMATION

Supplemental information can be found online at https://doi.org/10.1016/j.isci.2024.110489.

ACKNOWLEDGMENTS

The work was supported by University of Utah startup funds, the NIH (R01EY026924 and R01NS113073, to B.N.), an NIH Core grant (EY014800), and an unrestricted grant from Research to Prevent Blindness, Inc. (New York, NY) to the Department of Ophthalmology and Visual Sciences, University of Utah.

AUTHOR CONTRIBUTIONS

M.R. analyzed the data, B.N. collected the data, B.N. and Z.B. designed the experiment, B.N., Z.B., M.R.D., and M.R. designed the analysis plan, K.C., M.R., and B.N. wrote the manuscript, Z.B, M.R.D. and B.N. Supervised the study. All authors reviewed and approved the final version.

DECLARATION OF INTERESTS

Authors declare no competing interests.

Received: August 10, 2023
Revised: January 3, 2024
Accepted: July 9, 2024
Published: July 11, 2024

REFERENCES

1. D'Esposito, M., and Postle, B. (2015). The Cognitive Neuroscience of Working Memory. Annu. Rev. Psychol. *66*, 115–142. https://doi.org/10.1146/annurev-psych-010814-015031.
2. Luck, S.J., and Vogel, E.K. (2013). Visual working memory capacity: from psychophysics and neurobiology to individual differences. Trends Cogn. Sci. *17*, 391–400. https://doi.org/10.1016/j.tics.2013.06.006.
3. Unsworth, N., Fukuda, K., Awh, E., and Vogel, E.K. (2015). Working memory delay activity predicts individual differences in cognitive abilities. J. Cogn. Neurosci. *27*, 853–865. https://doi.org/10.1162/jocn_a_00765.
4. Teng, C., and Kravitz, D.J. (2019). Visual working memory directly alters perception. Nat. Hum. Behav. *3*, 827–836.
5. Awh, E., Jonides, J., and Reuter-Lorenz, P.A. (1998). Rehearsal in spatial working memory. J. Exp. Psychol. Hum. Percept. Perform. *24*, 780–790.
6. Constantinidis, C., and Klingberg, T. (2016). The neuroscience of working memory capacity and training. Nat. Rev. Neurosci. *17*, 438–449. https://doi.org/10.1038/nrn.2016.43.
7. Rosenberg, M.D., Martinez, S.A., Rapuano, K.M., Conley, M.I., Cohen, A.O., Cornejo, M.D., Donald, J., Hagler, J., Meredith, W.J., Anderson, K.M., et al. (2020). Behavioral and Neural Signatures of Working Memory in Childhood. J. Neurosci. *40*, 5090–5104. https://doi.org/10.1523/JNEUROSCI.2841-19.2020.
8. Brockhoff, L., Vetter, L., Bruchmann, M., Schindler, S., Moeck, R., and Straube, T. (2023). The effects of visual working memory load on detection and neural processing of task-unrelated auditory stimuli. Sci. Rep. *13*, 4342. https://doi.org/10.1038/s41598-023-31132-7.
9. Fuster, J.M., and Alexander, G.E. (1971). Neuron activity related to short-term memory. Science *173*, 652–654. https://doi.org/10.1126/science.173.3997.652.

10. Chelazzi, L., Duncan, J., Miller, E.K., and Desimone, R. (1998). Responses of neurons in inferior temporal cortex during memory-guided visual search. J. Neurophysiol. *80*, 2918–2940.
11. Chelazzi, L., Miller, E.K., Duncan, J., and Desimone, R. (2001). Responses of neurons in macaque area V4 during memory-guided visual search. Cereb. Cortex *11*, 761–772. https://doi.org/10.1093/cercor/11.8.761.
12. Mendoza-Halliday, D., Torres, S., and Martinez-Trujillo, J.C. (2014). Sharp emergence of feature-selective sustained activity along the dorsal visual pathway. Nat. Neurosci. *17*, 1255–1262.
13. Zaksas, D., and Pasternak, T. (2006). Directional Signals in the Prefrontal Cortex and in Area MT during a Working Memory for Visual Motion Task. J. Neurosci. *26*, 11726–11742. https://doi.org/10.1523/JNEUROSCI.3420-06.2006.
14. Lee, H., Simpson, G.V., Logothetis, N.K., and Rainer, G. (2005). Phase locking of single neuron activity to theta oscillations during working memory in monkey extrastriate visual cortex. Neuron *45*, 147–156.
15. Leavitt, M.L., Mendoza-Halliday, D., and Martinez-Trujillo, J.C. (2017). Sustained Activity Encoding Working Memories: Not Fully Distributed. Trends Neurosci. *40*, 328–346. https://doi.org/10.1016/j.tins.2017.04.004.
16. van Kerkoerle, T., Self, M.W., and Roelfsema, P.R. (2017). Layer-specificity in the effects of attention and working memory on activity in primary visual cortex. Nat. Commun. *8*, 13804. https://doi.org/10.1038/ncomms13804.
17. Serences, J.T., Ester, E.F., Vogel, E.K., and Awh, E. (2009). Stimulus-specific delay activity in human primary visual cortex. Psychol. Sci. *20*, 207–214. https://doi.org/10.1111/j.1467-9280.2009.02276.x.
18. Ester, E.F., Serences, J.T., and Awh, E. (2009). Spatially global representations in human primary visual cortex during working memory maintenance. J. Neurosci. *29*, 15258–15265. https://doi.org/10.1523/JNEUROSCI.4388-09.2009.
19. Harrison, S.A., and Tong, F. (2009). Decoding reveals the contents of visual working memory in early visual areas. Nature *458*, 632–635. https://doi.org/10.1038/nature07832.
20. Xing, Y., Ledgeway, T., McGraw, P.V., and Schluppeck, D. (2013). Decoding working memory of stimulus contrast in early visual cortex. J. Neurosci. *33*, 10301–10311. https://doi.org/10.1523/JNEUROSCI.3754-12.2013.
21. Christophel, T.B., Hebart, M.N., and Haynes, J.-D. (2012). Decoding the contents of visual short-term memory from human visual and parietal cortex. J. Neurosci. *32*, 12983–12989. https://doi.org/10.1523/JNEUROSCI.0184-12.2012.
22. Zaksas, D., Bisley, J.W., and Pasternak, T. (2001). Motion information is spatially localized in a visual working-memory task. J. Neurophysiol. *86*, 912–921. https://doi.org/10.1152/jn.2001.86.2.912.
23. Pasternak, T., and Zaksas, D. (2003). Stimulus specificity and temporal dynamics of working memory for visual motion. J. Neurophysiol. *90*, 2757–2762. https://doi.org/10.1152/jn.00422.2003.
24. Wimmer, K., Spinelli, P., and Pasternak, T. (2016). Prefrontal Neurons Represent Motion Signals from Across the Visual Field But for Memory-Guided Comparisons Depend on Neurons Providing These Signals. J. Neurosci. *36*, 9351–9364. https://doi.org/10.1523/JNEUROSCI.0843-16.2016.
25. Super, H., Spekreijse, H., and Lamme, V.A.F. (2001). A neural correlate of working memory in the monkey primary visual cortex. Science *293*, 120–124.
26. Scott, H., Wimmer, K., Pasternak, T., and Snyder, A.C. (2023). Altered task demands lead to a division of labour for sensory and cognitive processing in the middle temporal area. Eur. J. Neurosci. *57*, 1561–1576. https://doi.org/10.1111/ejn.15964.
27. Rose, N.S., LaRocque, J.J., Riggall, A.C., Gosseries, O., Starrett, M.J., Meyering, E.E., and Postle, B.R. (2016). Reactivation of latent working memories with transcranial magnetic stimulation. Science *354*, 1136–1139. https://doi.org/10.1126/science.aah7011.
28. Stokes, M.G. (2015). "Activity-silent" working memory in prefrontal cortex: a dynamic coding framework. Trends Cogn. Sci. *19*, 394–405. https://doi.org/10.1016/j.tics.2015.05.004.
29. Mongillo, G., Barak, O., and Tsodyks, M. (2008). Synaptic theory of working memory. Science *319*, 1543–1546. https://doi.org/10.1126/science.1150769.
30. Spaak, E., Watanabe, K., Funahashi, S., and Stokes, M.G. (2017). Stable and Dynamic Coding for Working Memory in Primate Prefrontal Cortex. J. Neurosci. *37*, 6503–6516. https://doi.org/10.1523/JNEUROSCI.3364-16.2017.
31. Cavanagh, S.E., Towers, J.P., Wallis, J.D., Hunt, L.T., and Kennerley, S.W. (2018). Reconciling persistent and dynamic hypotheses of working memory coding in prefrontal cortex. Nat. Commun. *9*, 3498. https://doi.org/10.1038/s41467-018-05873-3.
32. Mozumder, R., and Constantinidis, C. (2023). Single-neuron and population measures of neuronal activity in working memory tasks. J. Neurophysiol. *130*, 694–705. https://doi.org/10.1152/jn.00245.2023.
33. Oberauer, K., and Awh, E. (2022). Is There an Activity-silent Working Memory? J. Cogn. Neurosci. *34*, 2360–2374. https://doi.org/10.1162/jocn_a_01917.
34. Barbosa, J., Lozano-Soldevilla, D., and Compte, A. (2021). Pinging the brain with visual impulses reveals electrically active, not activity-silent, working memories. PLoS Biol. *19*, e3001436. https://doi.org/10.1371/journal.pbio.3001436.
35. Bao, Q., Zhang, H., Wang, Y., Ni, Z., Yan, Y., Shen, Z.X., Loh, K.P., and Tang, D.Y. (2009). Atomic-layer graphene as a saturable absorber for ultrafast pulsed lasers. Adv. Funct. Mater. *19*, 3077–3083.
36. Li, S., Constantinidis, C., and Qi, X.-L. (2021). Drifts in Prefrontal and Parietal Neuronal Activity Influence Working Memory Judgments. Cereb. Cortex *31*, 3650–3664. https://doi.org/10.1093/cercor/bhab038.
37. Stroud, J.P., Watanabe, K., Suzuki, T., Stokes, M.G., and Lengyel, M. (2023). Optimal information loading into working memory explains dynamic coding in the prefrontal cortex. Proc. Natl. Acad. Sci. USA *120*, e2307991120. https://doi.org/10.1073/pnas.2307991120.
38. Wolff, M.J., Jochim, J., Akyürek, E.G., Buschman, T.J., and Stokes, M.G. (2020). Drifting codes within a stable coding scheme for working memory. PLoS Biol. *18*, e3000625. https://doi.org/10.1371/journal.pbio.3000625.
39. Kamiński, J., and Rutishauser, U. (2020). Between persistently active and activity-silent frameworks: novel vistas on the cellular basis of working memory. Ann. N. Y. Acad. Sci. *1464*, 64–75. https://doi.org/10.1111/nyas.14213.
40. Sreenivasan, K.K., Curtis, C.E., and D'Esposito, M. (2014). Revisiting the role of persistent neural activity during working memory. Trends Cogn. Sci. *18*, 82–89. https://doi.org/10.1016/j.tics.2013.12.001.
41. Riggall, A.C., and Postle, B.R. (2012). The relationship between working memory storage and elevated activity as measured with functional magnetic resonance imaging. J. Neurosci. *32*, 12990–12998. https://doi.org/10.1523/JNEUROSCI.1892-12.2012.
42. Buschman, T.J., and Miller, E.K. (2022). Working Memory Is Complex and Dynamic, Like Your Thoughts. J. Cogn. Neurosci. *35*, 17–23. https://doi.org/10.1162/jocn_a_01940.
43. Lansner, A., Fiebig, F., and Herman, P. (2023). Fast Hebbian plasticity and working memory. Curr. Opin. Neurobiol. *83*, 102809. https://doi.org/10.1016/j.conb.2023.102809.
44. Beukers, A.O., Buschman, T.J., Cohen, J.D., and Norman, K.A. (2021). Is Activity Silent Working Memory Simply Episodic Memory? Trends Cogn. Sci. *25*, 284–293. https://doi.org/10.1016/j.tics.2021.01.003.
45. Bahmani, Z., Daliri, M.R., Merrikhi, Y., Clark, K., and Noudoost, B. (2018). Working memory enhances cortical representations via spatially specific coordination of spike times. Neuron *97*, 967–979.e6.
46. Merrikhi, Y., Clark, K., Albarran, E., Parsa, M., Zirnsak, M., Moore, T., and Noudoost, B. (2017). Spatial working memory alters the efficacy of input to visual cortex. Nat. Commun. *8*, 15041.
47. Merrikhi, Y., Clark, K., and Noudoost, B. (2018). Concurrent influence of top-down and bottom-up inputs on correlated activity of Macaque extrastriate neurons. Nat. Commun. *9*, 5393. https://doi.org/10.1038/s41467-018-07816-4.
48. Gayet, S., Guggenmos, M., Christophel, T.B., Haynes, J.-D., Paffen, C.L.E., Van der Stigchel, S., and Sterzer, P. (2017). Visual Working Memory Enhances the Neural Response to Matching Visual Input. J. Neurosci. *37*, 6638–6647. https://doi.org/10.1523/JNEUROSCI.3418-16.2017.
49. Rapela, J., Westerfield, M., Townsend, J., and Makeig, S. (2016). A new foreperiod effect on single-trial phase coherence. Part I: existence and relevance. Preprint at arXiv. https://doi.org/10.48550/arXiv.1611.00313.
50. Comeaux, P., Clark, K., and Noudoost, B. (2023). A recruitment through coherence theory of working memory. Prog. Neurobiol. *228*, 102491. https://doi.org/10.1016/j.pneurobio.2023.102491.
51. Abdalaziz, M., Redding, Z.V., and Fiebelkorn, I.C. (2023). Rhythmic temporal coordination of neural activity prevents representational conflict during working memory. Curr. Biol. *33*, 1855–1863.e3. https://doi.org/10.1016/j.cub.2023.03.088.
52. Jun, N.Y., Ruff, D.A., Kramer, L.E., Bowes, B., Tokdar, S.T., Cohen, M.R., and Groh, J.M. (2022). Coordinated multiplexing of information about separate objects in visual cortex. Elife *11*, e76452. https://doi.org/10.7554/eLife.76452.
53. Caruso, V.C., Mohl, J.T., Glynn, C., Lee, J., Willett, S.M., Zaman, A., Ebihara, A.F., Estrada, R., Freiwald, W.A., Tokdar, S.T., and

Groh, J.M. (2018). Single neurons may encode simultaneous stimuli by switching between activity patterns. Nat. Commun. *9*, 2715. https://doi.org/10.1038/s41467-018-05121-8.

54. Williams, G.V., and Goldman-Rakic, P.S. (1995). Modulation of memory fields by dopamine D1 receptors in prefrontal cortex. Nature *376*, 572–575. https://doi.org/10.1038/376572a0.
55. Sawaguchi, T., and Iba, M. (2001). Prefrontal cortical representation of visuospatial working memory in monkeys examined by local inactivation with muscimol. J. Neurophysiol. *86*, 2041–2053. https://doi.org/10.1152/jn.2001.86.4.2041.
56. Steinmetz, N.A., and Moore, T. (2014). Eye movement preparation modulates neuronal responses in area V4 when dissociated from attentional demands. Neuron *83*, 496–506. https://doi.org/10.1016/j.neuron.2014.06.014.
57. Bahmani, Z., Clark, K., Merrikhi, Y., Mueller, A., Pettine, W., Isabel Vanegas, M., Moore, T., and Noudoost, B. (2019). Prefrontal Contributions to Attention and Working Memory. Curr. Top. Behav. Neurosci. *41*, 129–153. https://doi.org/10.1007/7854_2018_74.
58. Noudoost, B., Chang, M.H., Steinmetz, N.A., and Moore, T. (2010). Top-down control of visual attention. Curr. Opin. Neurobiol. *20*, 183–190.
59. Rezayat, E., Dehaqani, M.-R.A., Clark, K., Bahmani, Z., Moore, T., and Noudoost, B. (2021). Frontotemporal coordination predicts working memory performance and its local neural signatures. Nat. Commun. *12*, 1103. https://doi.org/10.1038/s41467-021-21151-1.
60. Tallon-Baudry, C., Mandon, S., Freiwald, W.A., and Kreiter, A.K. (2004). Oscillatory synchrony in the monkey temporal lobe correlates with performance in a visual short-term memory task. Cereb. Cortex *14*, 713–720. https://doi.org/10.1093/cercor/bhh031.
61. Liebe, S., Hoerzer, G.M., Logothetis, N.K., and Rainer, G. (2012). Theta coupling between V4 and prefrontal cortex predicts visual short-term memory performance. Nat. Neurosci. *15*, 456. https://doi.org/10.1038/nn.3038.
62. Daume, J., Gruber, T., Engel, A.K., and Friese, U. (2017). Phase-Amplitude Coupling and Long-Range Phase Synchronization Reveal Frontotemporal Interactions during Visual Working Memory. J. Neurosci. *37*, 313–322. https://doi.org/10.1523/JNEUROSCI.2130-16.2016.
63. Bastos, A.M., Vezoli, J., Bosman, C.A., Schoffelen, J.-M., Oostenveld, R., Dowdall, J.R., De Weerd, P., Kennedy, H., and Fries, P. (2015). Visual areas exert feedforward and feedback influences through distinct frequency channels. Neuron *85*, 390–401. https://doi.org/10.1016/j.neuron.2014.12.018.
64. Buffalo, E.A., Fries, P., Landman, R., Buschman, T.J., and Desimone, R. (2011). Laminar differences in gamma and alpha coherence in the ventral stream. Proc. Natl. Acad. Sci. USA *108*, 11262–11267. https://doi.org/10.1073/pnas.1011284108.
65. Michalareas, G., Vezoli, J., van Pelt, S., Schoffelen, J.-M., Kennedy, H., and Fries, P. (2016). Alpha-Beta and Gamma Rhythms Subserve Feedback and Feedforward Influences among Human Visual Cortical Areas. Neuron *89*, 384–397. https://doi.org/10.1016/j.neuron.2015.12.018.
66. van Kerkoerle, T., Self, M.W., Dagnino, B., Gariel-Mathis, M.-A., Poort, J., van der Togt, C., and Roelfsema, P.R. (2014). Alpha and gamma oscillations characterize feedback and feedforward processing in monkey visual cortex. Proc. Natl. Acad. Sci. USA *111*, 14332–14341. https://doi.org/10.1073/pnas.1402773111.
67. Fries, P., Reynolds, J.H., Rorie, A.E., and Desimone, R. (2001). Modulation of oscillatory neuronal synchronization by selective visual attention. Science *291*, 1560–1563. https://doi.org/10.1126/science.1055465.
68. Fries, P., Womelsdorf, T., Oostenveld, R., and Desimone, R. (2008). The effects of visual stimulation and selective visual attention on rhythmic neuronal synchronization in macaque area V4. J. Neurosci. *28*, 4823–4835. https://doi.org/10.1523/JNEUROSCI.4499-07.2008.
69. Rohenkohl, G., Bosman, C.A., and Fries, P. (2018). Gamma Synchronization between V1 and V4 Improves Behavioral Performance. Neuron *100*, 953–963.e3. https://doi.org/10.1016/j.neuron.2018.09.019.
70. Bastos, A.M., Vezoli, J., and Fries, P. (2015). Communication through coherence with inter-areal delays. Curr. Opin. Neurobiol. *31*, 173–180. https://doi.org/10.1016/j.conb.2014.11.001.
71. Fries, P. (2015). Rhythms for cognition: communication through coherence. Neuron *88*, 220–235.
72. Foxe, J.J., and Snyder, A.C. (2011). The Role of Alpha-Band Brain Oscillations as a Sensory Suppression Mechanism during Selective Attention. Front. Psychol. *2*, 154. https://doi.org/10.3389/fpsyg.2011.00154.
73. Rezayat, E., Clark, K., Dehaqani, M.-R.A., and Noudoost, B. (2021). Dependence of Working Memory on Coordinated Activity Across Brain Areas. Front. Syst. Neurosci. *15*, 787316. https://doi.org/10.3389/fnsys.2021.787316.
74. Miller, E.K., Lundqvist, M., and Bastos, A.M. (2018). Working Memory 2.0. Neuron *100*, 463–475. https://doi.org/10.1016/j.neuron.2018.09.023.
75. Lee, J., Williford, T., and Maunsell, J.H.R. (2007). Spatial Attention and the Latency of Neuronal Responses in Macaque Area V4. J. Neurosci. *27*, 9632–9637. https://doi.org/10.1523/JNEUROSCI.2734-07.2007.
76. Galashan, F.O., Saßen, H.C., Kreiter, A.K., and Wegener, D. (2013). Monkey area MT latencies to speed changes depend on attention and correlate with behavioral reaction times. Neuron *78*, 740–750. https://doi.org/10.1016/j.neuron.2013.03.014.
77. Ito, J., Joana, C., Yamane, Y., Fujita, I., Tamura, H., Maldonado, P.E., and Grün, S. (2022). Latency shortening with enhanced sparseness and responsiveness in V1 during active visual sensing. Sci. Rep. *12*, 6021. https://doi.org/10.1038/s41598-022-09405-4.

STAR★METHODS

KEY RESOURCES TABLE

REAGENT or RESOURCE	SOURCE	IDENTIFIER
Deposited data		
Data	GIN	https://gin.g-node.org/KClark/MT_MGSprobe.git
Code	GitHub	https://doi.org/10.5281/zenodo.12117406
Software and algorithms		
MATLAB	MathWorks	https://www.mathworks.com/; RRID: SCR_001622
Plexon offline sorter	Plexon	https://plexon.com/products/

RESOURCE AVAILABILITY

Lead contact

Requests for further information and resources should be directed to and will be fulfilled by the Lead Contact, Behrad Noudoost (behrad.noudoost@utah.edu).

Materials availability

This study did not generate new unique reagents.

Data and code availability

- Data have been deposited at GIN and are publicly available as of the date of publication. Repository link is listed in the key resources table.
- All original code has been deposited at GitHub and is publicly available as of the date of publication. DOI is listed in the key resources table.
- Any additional information required to reanalyze the data reported in this paper is available from the lead contact upon request.

EXPERIMENTAL MODEL AND STUDY PARTICIPANT DETAILS

General and surgical procedures

The data were collected at Montana State University and were used in previous publications.[45,46] Two adult male rhesus monkeys (Macaca mulatta) were used in this study. All experimental procedures were in accordance with the National Institutes of Health Guide for the Care and Use of Laboratory Animals and the Society for Neuroscience Guidelines and Policies. The protocols for all experimental, surgical, and behavioral procedures were approved by the Montana State University Institutional Animal Care and Use Committee. All surgical procedures were carried out under Isoflurane anesthesia and strict aseptic conditions. Prior to undergoing behavioral training, each animal was implanted with a stainless steel headpost (Gray Matter Research, Bozeman MT), attached to the skull using orthopedic titanium screws and dental acrylic. Following behavioral training, custom-made PEEK recording chambers (interior 22 × 22 mm) were mounted on the skull and affixed with dental acrylic. Within the chambers two 22 × 22 mm craniotomies were performed above the prefrontal and extrastriate visual areas (prefrontal chambers were centered at 42 mm A/P, 23 mm M/L and 28 mm A/P, 23 mm M/L; extrastriate craniotomies were centered at −6 mm A/P, 23 mm M/L and −13 mm A/P, 23 mm M/L).

Behavioral monitoring

Animals were seated in a custom-made primate chair, with their head restrained and a tube to deliver juice rewards placed in their mouth. Eye position was monitored with an infrared optical eye tracking system (EyeLink 1000 Plus Eye Tracker, SR Research Ltd, Ottawa CA), with a resolution of <0.01° RMS; eye position was monitored and stored at 2 kHz. The EyeLink PM-910 Illuminator Module and EyeLink 1000 Plus Camera (SR Research Ltd, Ottawa CA) were mounted above the monkey's head, and captured eye movements via an angled infrared mirror. Juice was delivered via a syringe pump and the Syringe PumpPro software (NE-450 1L- X2, New Era Pump Systems, Inc., Farmingdale NY). Stimulus presentation and juice delivery were controlled using custom software, written in MATLAB using the MonkeyLogic toolbox (Asaad et al., 2013). Visual stimuli were presented on an LED-lit monitor (Asus VG248QE: 24in, resolution 1920 × 1080, 144 Hz refresh rate), positioned 28.5 cm in front of the animal's eyes. A photodiode (OSRAM Opto Semiconductors, Sunnyvale CA) was used to record the actual time of stimulus appearance on the monitor, with a continuous signal sampled and stored at 32 kHz.

Behavioral tasks

Eye calibration

The fixation point, a ~1 dva white circle, appeared in the center of the screen, and the monkey maintained its fixation within a ±1.5 dva window for 1.5 s. For eye calibration, the fixation point could appear either centrally or offset by 10 dva in the vertical or horizontal axis. The monkey was rewarded for maintaining fixation.

Preliminary receptive field mapping

Preliminary receptive field mapping was conducted by having the monkey fixate within a ±1.5 dva window around the central fixation point, while ~2.5 × 4 dva white bars swept in 8 directions (4 orientations) across the approximate location of the neuron's receptive field. Responses from the recording site were monitored audibly and visually by the experimenter, and the approximate boundaries of the receptive field were noted for the positioning of stimuli in subsequent behavioral tasks.

Memory guided saccade task with visual probes

Monkeys fixated within a ±1.5 dva window around the central fixation point. After 1 s of fixation, a 1.35 dva square target was presented and remained onscreen for 1 s. The animal then remembered the target location while maintaining fixation for 1 s (memory period) before the central fixation point was removed. The animal then had 500 ms to move his eyes to a ±4 dva window around the previous target location, and remain fixating there for 200 ms to receive a reward. A series of brief (200 ms) visual probes (~1 dva white circles) appeared in a 7 × 7 dva grid of locations (1–2.5 dva spacing), both before target presentation (fixation receptive field mapping) and during the memory period (memory period receptive field mapping). Four probes were presented in succession on each trial, with an inter-probe interval of 200 ms. This 7 × 7 grid of probes was positioned to overlap with the receptive field of the recorded neuron based on the preliminary receptive field mapping described above. The location of the remembered target could vary with respect to the receptive field of recorded neurons (see Figure 1B).

Neurophysiological recording

Neurophysiological data were recorded from two adult male rhesus monkeys (Macaca mulatta) across 18 sessions (7 sessions from monkey 1 and 11 sessions from monkey 2). This dataset was previously used in Bahmani et al., 2018.

The electrode was mounted on the recording chamber and positioned within the craniotomy area using a Narishige two-axis platform allowing continuous adjustment of the electrode position. For array electrode recordings a 28-gauge guide tube was lowered as described, and the 16-channel linear array electrode (V-probe, Plexon, Inc., Dallas, TX; distance between electrode contacts was 150mm) was advanced into the brain using the hydraulic microdrive. The array electrode was connected to a headstage pre-amplifier (Neuralynx, Inc., Bozeman MT). Neuralynx Digital Lynx SX and associated software were used for data acquisition. Spike waveforms and continuous data were digitized and stored at 32 kHz for offline spike sorting and data analysis. Spike waveforms were sorted manually, and the quality of isolations for simultaneously recorded neurons confirmed using a support vector machine classifier (see Bahmani et al. 2018 for analysis). Area MT was identified based on stereotaxic location, position relative to nearby sulci, patterns of gray and white matter, and response properties of units encountered. The location of brain areas within the recording chamber was verified via single-electrode exploration prior to beginning data collection with the electrode arrays.

METHOD DETAILS

Data analysis

288 LFP channels were recorded across 18 recording sessions. 205 channels had multi-unit receptive fields, and of these 137 channels also had well-isolated single unit receptive fields. 83 channels were excluded from further analysis due to a lack of strong visual signals.

All analyses were carried out using MATLAB. All population statistics are reported as mean ± SEM (standard error of mean). Statistics are all Wilcoxon signed rank, unless otherwise mentioned.

ITC method

The LFP signal was resampled at 1000 Hz and normalized by subtracting the mean waveform and dividing the result by the standard deviation over trials. ITC calculations use a matrix of LFP data, where each row represents a trial and each column represents a time point. We only used the LFP in response to the probes appearing in optimal locations, defined as the probe locations evoking a firing rate response of more than 60 percent of the maximum response of the neuron to all probes in the fixation period (responses 30–150 ms after probe onset). To use ITC to estimate the time of synaptic inputs, a frequency must be selected for the analysis. As shown in Figures 1C and 1D, the LFP event-related potential had power in the Alpha-Beta band (5–30 Hz), therefore, the center frequency for further calculations was set to 15 Hz (spanning 5 Hz–25 Hz based on wavelet parameters). For ITC calculations, the normalized LFP was convolved with a complex Morlet wavelet, as here:

$$w(t, f_0) = A \,.exp\left(-\frac{Ct^2}{2\sigma_t^2}\right).exp\,(2\pi i f_0 t),$$

where $A = (\sigma_t\sqrt{\pi})^{-1/2}$ is a normalization factor, t is the time, f_0 is center frequency of the wavelet, $C = 3$ is the number of wavelet cycles, and σ_t is the standard deviation of the Gaussian taper. We used wavelets with $\sigma_t = 1/\pi f_0$, truncated at $\pm 3\,\sigma_t$, and the length of wavelet support was

fixed at −250 ms–250 ms (in other words, wavelets that are broad in the frequency domain and short in the time domain, in order to get better time resolution). The results of Figures 2E and 2F are replicated in Figure S9 using a shorter wavelet support, from −100 ms to 100 ms. Since the wavelet convolution was symmetric, no phase delays were brought about. Signal amplitude and phase were delivered for each time and frequency via the wavelet transform. When phases are represented as unit-length complex vectors, the ITC is defined as the vector average across trials. ITC has a range of zero to one, with zero denoting random phases (no coherence) and one denoting phases that are identical across all trials (full coherence). A randomly sampled ITC for comparison was obtained by randomly sampling ITCs at different times; the sampling procedure was repeated 1000 times, and the average of these values was defined as the randomly sampled ITC. The first time point for which the actual ITC values significantly increased from the randomly sampled ITC was used to define the EIT.

EIT calculations

EIT was calculated separately for different conditions: during fixation, memory In, memory Out, and memory Flank conditions. There were three potential memory locations in or near the estimated MT receptive field (black, red and purple dot in Figure 1B). receptive field mapping was performed based on spiking responses to probes during the fixation period (30–150 ms after probe onset), with memory conditions assigned during data analysis based on these receptive field maps. The "memory In" condition was when the memory cue appeared closest to the receptive field center (<3 dva), and the neuron was highly responsive to stimuli (>60% of the maximum response of the neuron to all probes). The condition with the cue furthest from the receptive field center was defined as the "Flank condition". The memory Out cue was in the opposite hemifield from the receptive field. Fixation period values were calculated separately for the In, Out, and Flank conditions.

The ITC technique is sensitive to the number of trials, so a bootstrap approach was employed to equalize the number of trials used in the ITC calculation for each condition. In this approach, a number of trials equal to the minimum available across conditions were randomly selected from each condition and used to calculate the ITC. This process was repeated 80 times, and the final result was calculated by averaging across all repetitions.

Baseline adjustment: We calculated the baseline ITC for each probe and memory condition. To calculate the adjusted ITC, we subtracted the average ITC in the 30 ms prior to probe onset from the subsequent ITC values. The pre-stimulus ITC is not essentially zero. This is due to the fact that the task has a specific sequence of events which induces some level of similarity in the ERP of various trials at each time within a condition. The baseline subtraction is meant to subtract this global coherence in order to enable us to identify the impact of probe presentation in various conditions. Probes evoked a significant increase in firing rate from 36 ms to 130 ms after probe onset for the memory In condition, and from 37 ms to 136 ms for the Fixation condition (Figure S10).

Phase variance

As an alternative method to measure input time based on changes in phase consistency after a stimulus, we looked at the variance of phase across trials over time relative to the stimulus. The LFP signal was first processed as described above for the ITC method, and then the variance of phase across trials was taken at each timepoint. High variance corresponds to phases being uniformly distributed across trials, and low variance corresponds to phases being more consistent across trials. Phase variance drops after stimulus onset (Figure S7A). We then calculated the EIT based on when the phase variance across trials reached 50% of its minimum (Figures S7B and S7C).

Fitted model

In order to predict memory input time, given fixation input time, distance from the receptive field center, and distance from the memorized location, we fit a polynomial of order 2 (using the *fit* MATLAB function) to the fixation and memory EITs, with EIT calculated for each set of four neighboring probe locations. Equation 1 describes this fitted model of order two as:

$$mt - ft = -2.88 + 0.81rf + 0.18ml - 0.019rf^2 - 0.017rf \times ml \quad \text{(Equation 1)}$$

Where *mt* is memory input time, *ft* is fixation input time, *rf* is probe set distance from the center of the fixation receptive field, and *ml* is probe set distance from the memorized location. *rf* and *ml* are fixed in the range of [0 to 15] and [0 to 30], respectively. R-squared of this model was 0.33.

QUANTIFICATION AND STATISTICAL ANALYSIS

Statistical analysis was performed using custom code written in MATLAB (MathWorks). Statistical details including means, *p*-values, exact value of n, and what n represents are described in the results; p and *n* values for plotted data are also shown on the relevant figure panel. All population statistics are reported as mean ± SE (standard error). Nonparametric statistical tests (Wilcoxon signed-rank for paired comparisons, Wilcoxon rank sum for unpaired comparisons) are used throughout for calculating *p* values.